

Supporting Information for:

**Disturbance of Intermolecular Forces: Eutectics as a New Tool for the
Preparation of Vapor-Phase Deposition Precursors**

Michael A. Land,^{*,†} Katherine N. Robertson,[‡] Jason A. C. Clyburne,[‡] and Seán T. Barry[†]

[†] *Department of Chemistry, Carleton University, 1125 Colonel By Drive, Ottawa, Ontario K1S 5B6, Canada*

[‡] *Department of Chemistry, Saint Mary's University, Halifax, Nova Scotia B3H 3C3, Canada*

*Corresponding Author. E-mail: Michael.land@carleton.ca

Contents

Experimental	2
Thermal Data (TGA and DSC)	4
NMR Spectroscopy	5
IR Spectroscopy	6
Powder X-ray Diffraction	7
Electrostatic Potential Maps	8
X-Ray Crystallography	9
References	30

Experimental

General Methods. All manipulations were performed under air-free conditions using either standard Schlenk techniques or in a nitrogen-filled (99.998% purity) MBraun glovebox. All reagents were purchased from Sigma-Aldrich and were used as received. $(^t\text{BuN})_2\text{MoCl}_2\cdot\text{dad}$ (**1**),¹ $[(^t\text{BuN})_2\text{MoCl}(\mu\text{-Cl})\cdot(^t\text{BuNH}_2)]_2$ (**2**),² and $(^t\text{BuN})_2\text{MoCl}_2\cdot\text{dme}$ (**3**)³ were prepared following known methods. All solvents (ACS reagent-grade) were purified using a MBraun Solvent Purification System and were stored over 4 Å molecular sieves. All glassware was oven-dried at 130 °C, for at least 3 hours, prior to use. ¹H NMR spectra were collected on a Bruker AVANCE 300 MHz spectrometer at room temperature and are referenced to residual solvent. C₆D₆ (99 atom % D) was purchased from Sigma-Aldrich and was degassed using freeze-pump-thaw cycles prior to being stored over 4 Å molecular sieves under nitrogen.

Method 1: Preparation of the Physical Mixtures of 1 and 2. Approximately 150 mg of material was ground together using a pestle and mortar. The composition of material depended on the mole fraction of interest. For example, for $\chi = 0.50$: 0.056 g (0.12 mmol) of **1** and 0.090 g (0.12 mmol) of **2** were ground together into a fine powder. The pale-orange or yellow powders were collected and used for further analysis. Eutectic mixture (**2:1₂**): EA calcd for C₆₀H₁₃₄Cl₈Mo₄N₁₄ [%]: C, 41.92; H, 7.86; N, 11.41; found [%]: C, 42.13; H, 8.18; N, 12.14.

Method 2: Preparation of the Physical Mixtures of 1 and 2. Approximately 150 mg of material was combined in a 20 mL scintillation vial. The composition depended on the mole fraction of interest ($\chi_2 = 0.25, 0.33, \text{ and } 0.50$). The powder was dissolved in 10 mL of Et₂O and was stirred at room temperature for 5 hours. The volatiles of the mixture were removed *in vacuo* and the resulting pale-orange solids were collected and analysed by DSC. The DSC traces resembled those prepared of the same mole fraction, prepared by Method 1.

Method 3: Preparation of the Physical Mixtures of 1 and 2. Solid samples of **1** and **2** were combined in a 20 mL scintillation vial. The composition depended on the mole fraction of interest ($\chi_2 = 0.25, 0.33, \text{ and } 0.50$). The two solid samples were gently mixed together with a spatula to try to evenly disperse them. The pale-orange solids were collected and analysed by DSC. The DSC traces resembled those prepared of the same mole fraction, prepared by Method 1, suggesting the phenomenon we observed was not due to mechanochemistry.

Sublimation of the Eutectic Mixture. A 0.110 g sample of the eutectic mixture (**2:1₂**, *e.g.*, 0.061 g (0.13 mmol) of **1** and 0.049 g (0.064 mmol) of **2**, prepared from grinding into a fine powder with a pestle and mortar) was sublimed under dynamic vacuum (100 °C, 40 mTorr) onto a water-cooled cold finger. The pale-orange sublimate was analysed using DSC and its melting point matched that of the eutectic mixture (113 °C) suggesting the mixture co-evaporates. The ¹H NMR spectrum of the sublimate was also consistent with a pure sample of **2:1₂** (Figure S4).

Crystallization of $[(^t\text{BuN})_2\text{MoCl}(\mu\text{-Cl})\cdot(^t\text{BuNH}_2)]_2\cdot 2[(^t\text{BuN})_2\text{MoCl}_2\cdot\text{dme}]$ (2:3₂**).** The dme adduct **3** (0.173 g, 0.434 mmol) was added to a suspension of the dimeric compound **2** (0.166 g, 0.217 mmol) in 7 mL of diethyl ether, immediately resulting in a pale-orange solution. The mixture was stirred at ambient temperature for 5 hours then the solution was then stored at -30 °C for 1 week resulting in a mixture of orange block crystals (**2**, CCDC: ZOBMIM²), thin yellow plate-like crystals of the co-crystal product (**2:3₂**), and yellow prisms (a new polymorph of **3**, see below). The crystalline products were carefully separated by hand; however, adequate combustion analyses could not be obtained due to contamination with the other components. Co-crystal (**2:3₂**):

EA calcd for $C_{48}H_{114}Cl_8Mo_4N_{10}O_4$ [%]: C, 36.89; H, 7.35; N, 8.96; found [%]: C, 35.21; H, 7.28; N, 9.12.

Differential Scanning Calorimetry. DSC experiments were performed with a TA Instruments Q100 instrument. The DSC was calibrated at the melting point of indium metal (156.6 °C). All DSC samples were hermetically sealed in aluminium pans inside a glovebox prior to analysis. All samples were heated to 400 °C with a ramp rate of 10 °C min⁻¹, using nitrogen (99.998% purity, 50 sccm) as the purge gas. The melting points were measured as the onset of the endothermic process and were also verified using an *ex situ* melting point apparatus. For mixtures that had two endothermic processes, the melting point was measured as the onset of the second endotherm as this would ensure the entire sample has melted. In all of the mixtures with two endotherms, the first endotherm occurs at 113(± 1) °C, further confirming the *solidus* temperature.

Thermogravimetric Analysis. TGA was performed on a TA Instruments Discovery TGA 55 instrument which was housed in a “chemical-free”, nitrogen-filled (99.998%) MBraun Labmaster 130 glovebox. 11 mg of analyte was placed in a platinum pan and was heated to 500 °C with a ramp rate of 10 °C min⁻¹, using nitrogen (99.999% purity, 60 sccm) as the purge gas. Platinum pans were cleaned by sequential sonication in glacial acetic acid then isopropanol, followed by heating until red-hot with a propane torch.

Powder X-ray Diffraction. X-ray diffraction measurements of the powder samples were collected on a Malvern PANalytical Empyrean X-ray diffractometer using Cu K α ($\lambda = 1.5406 \text{ \AA}$) radiation. A ~150 mg sample, which was ground into a fine powder with a pestle and mortar, was mounted in an aluminum holder on a glass slide and experiments were conducted in a 2θ range of 5-60° for 20 minutes.

Infrared Spectroscopy. IR spectroscopy was performed on a ABB Bomem MB100 FTIR with a resolution of 4 cm⁻¹. The IR spectra were collected as KBr pellets, which were prepared by combing the analyte and KBr in a pestle and mortar.

DFT Calculations. All calculations were performed using Gaussian 16, Rev A.03,⁴ and were carried out using the Cedar cluster, located at Simon Fraser University and maintained by the Digital Research Alliance of Canada. The X-ray crystal structures of **1**, **2**, and **3** were used as initial geometries and optimizations were performed with the BP86 density functional⁵ using the def2-SVP basis set,⁶ and showed zero negative frequencies. Single-point energy calculations were then performed with the BP86 density functional, the de2-TZVP basis set,⁶ and Grimme’s empirical atom-pairwise dispersion correction with Becke-Johnson damping [D3(BJ)].⁷ Electrostatic potential surfaces were generated using Multiwfn 3.7⁸ and were rendered using VMD 1.9.3.⁹

Thermal Data (DSC and TGA)

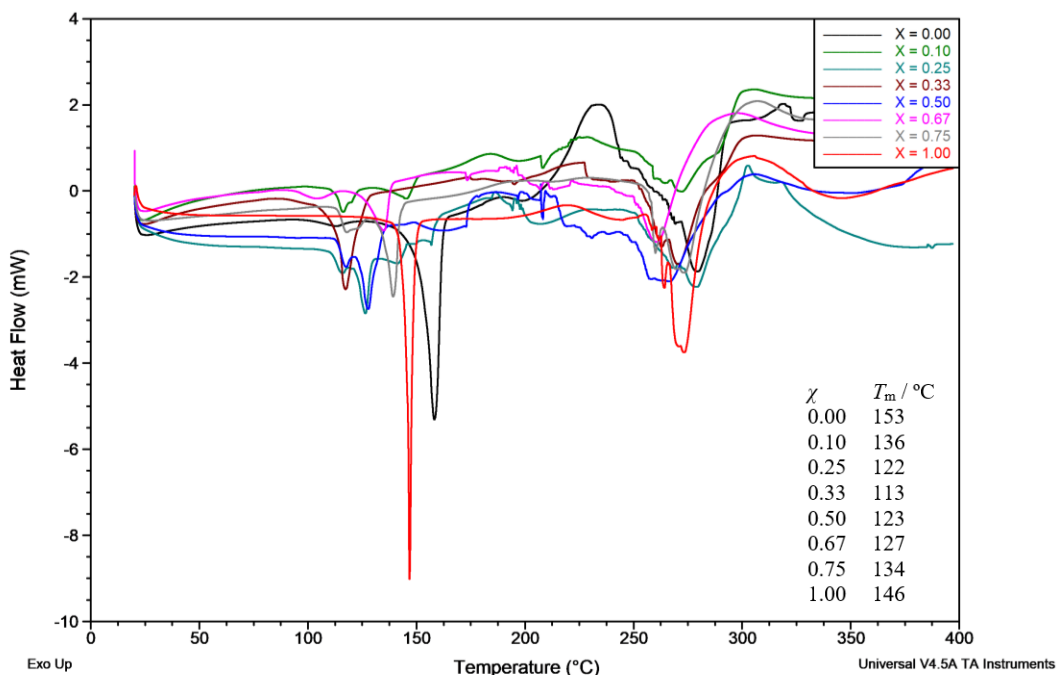


Figure S1: Differential scanning calorimetry plots of the physical mixtures of $(^t\text{BuN})_2\text{MoCl}_2\cdot\text{dad}$ (**1**) and $[(^t\text{BuN})_2\text{MoCl}(\mu\text{-Cl})\cdot(^t\text{BuNH}_2)]_2$ (**2**). Mole fraction is shown with respect to **2** (e.g., $\chi = 0.00$ for pure **1** and $\chi = 1.00$ for pure **2**).

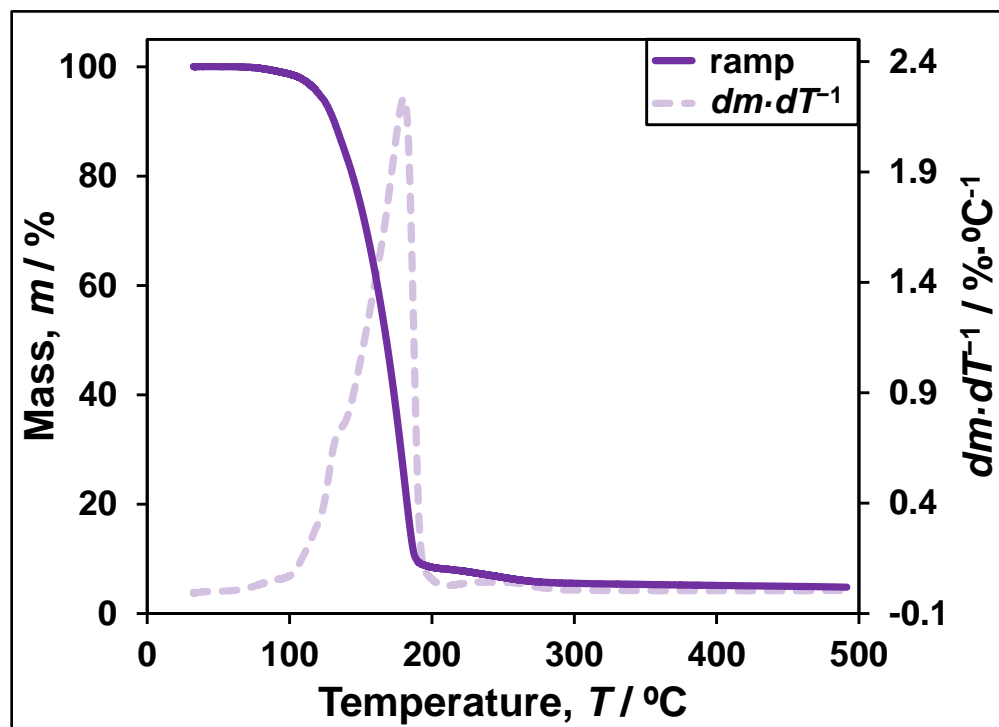


Figure S2: Thermogravimetric analysis of the eutectic mixture (**2:1**) with a heating rate of $10\text{ }^\circ\text{C}\cdot\text{min}^{-1}$ and a mass loading of 11.3 mg . The residual mass was 4.8% .

NMR Spectroscopy

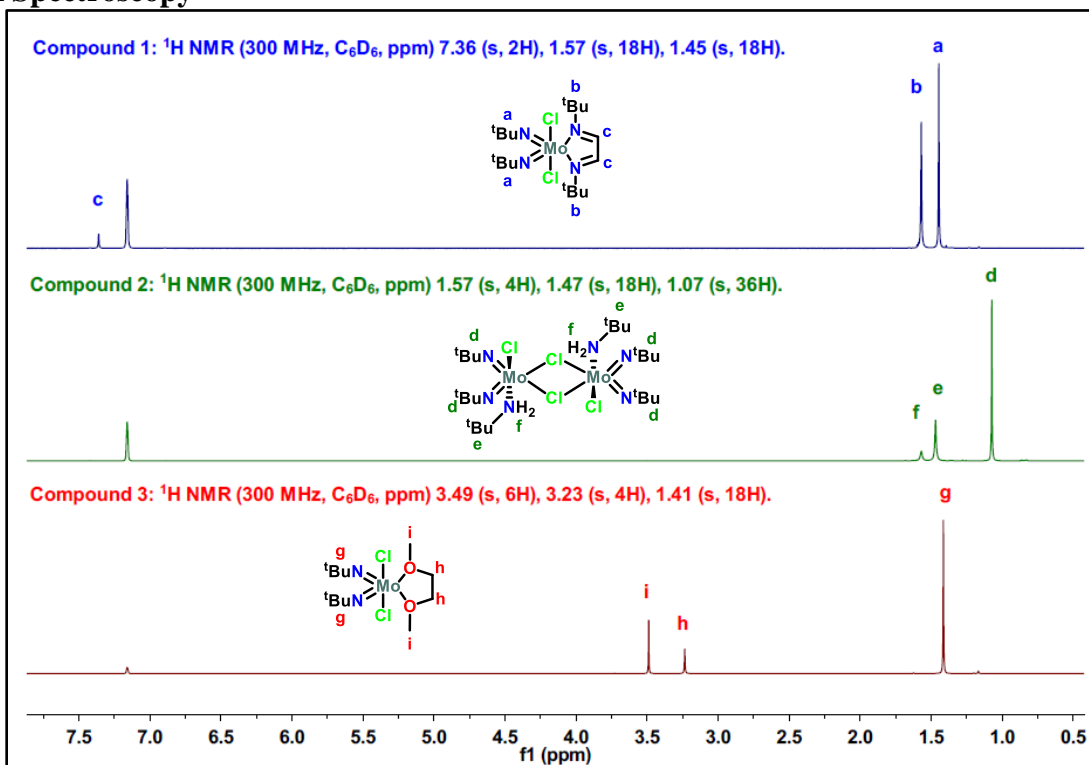


Figure S3: ^1H NMR spectra of **1** (top, blue), **2** (middle, green), and **3** (bottom, red), in C_6D_6 .

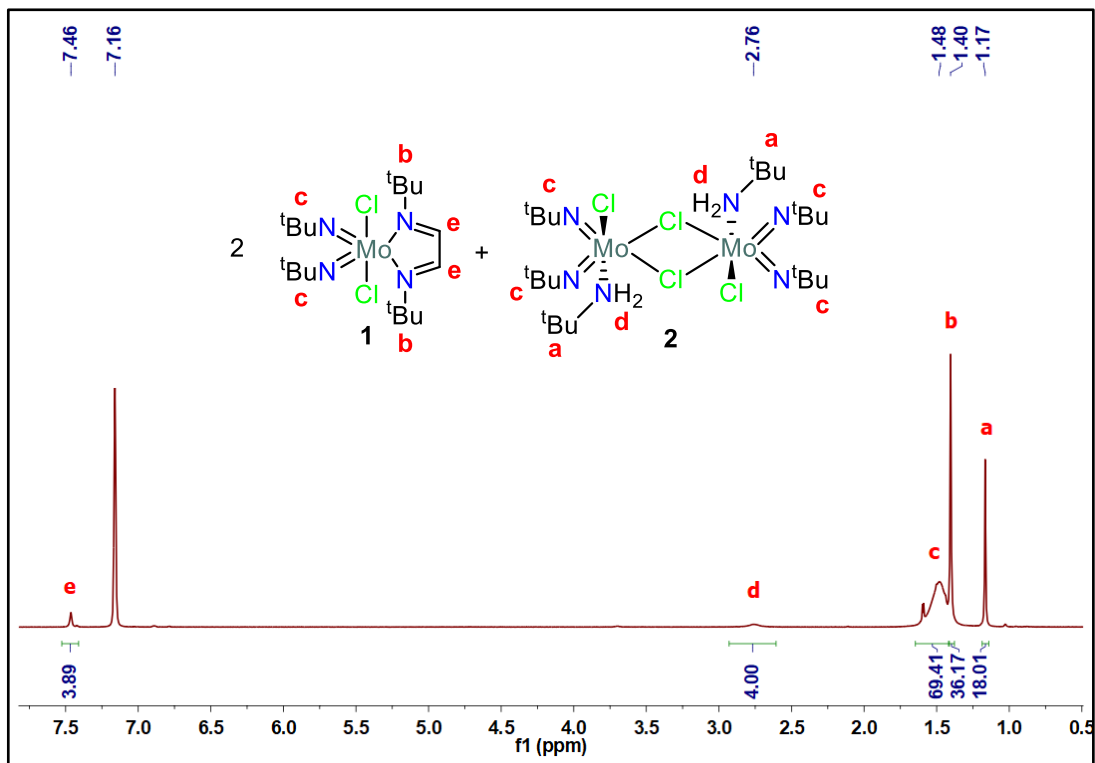


Figure S4: ^1H NMR spectrum of the eutectic mixture (**2**:**12**), prepared by Method 1, in C_6D_6 . An identical spectrum was also obtained when **2**:**12** was prepared by Method 2.

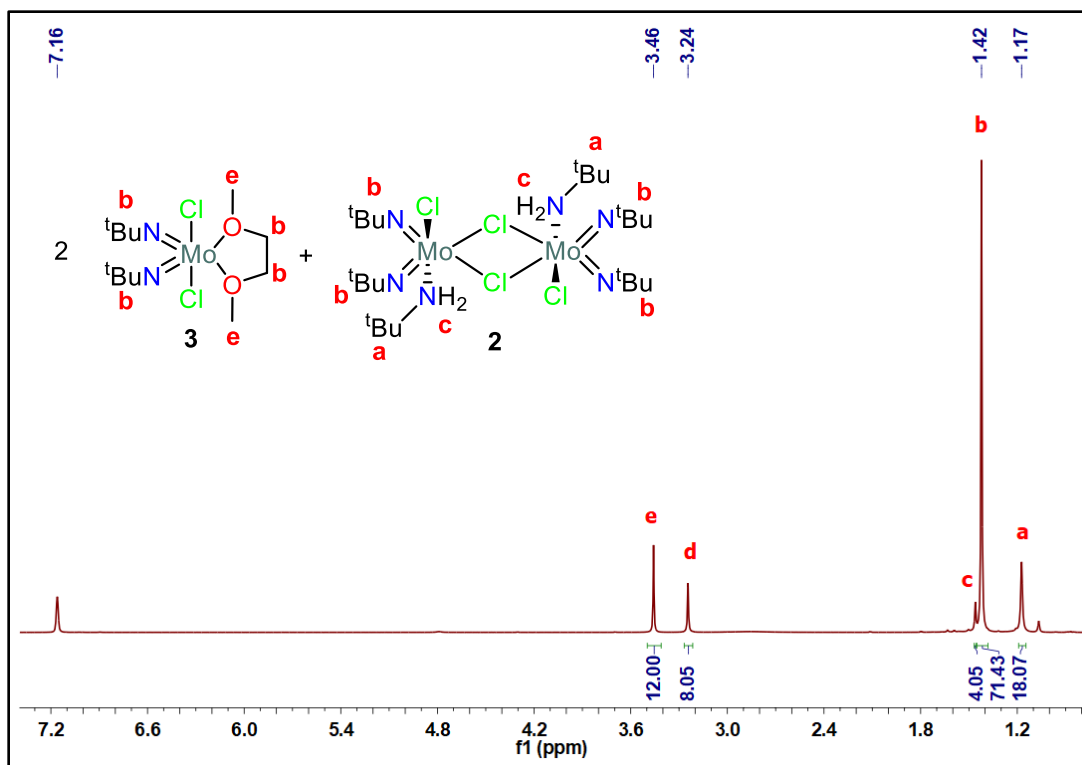


Figure S5: ^1H NMR spectrum of the co-crystal (**2:32**) in C_6D_6 .

IR Spectroscopy

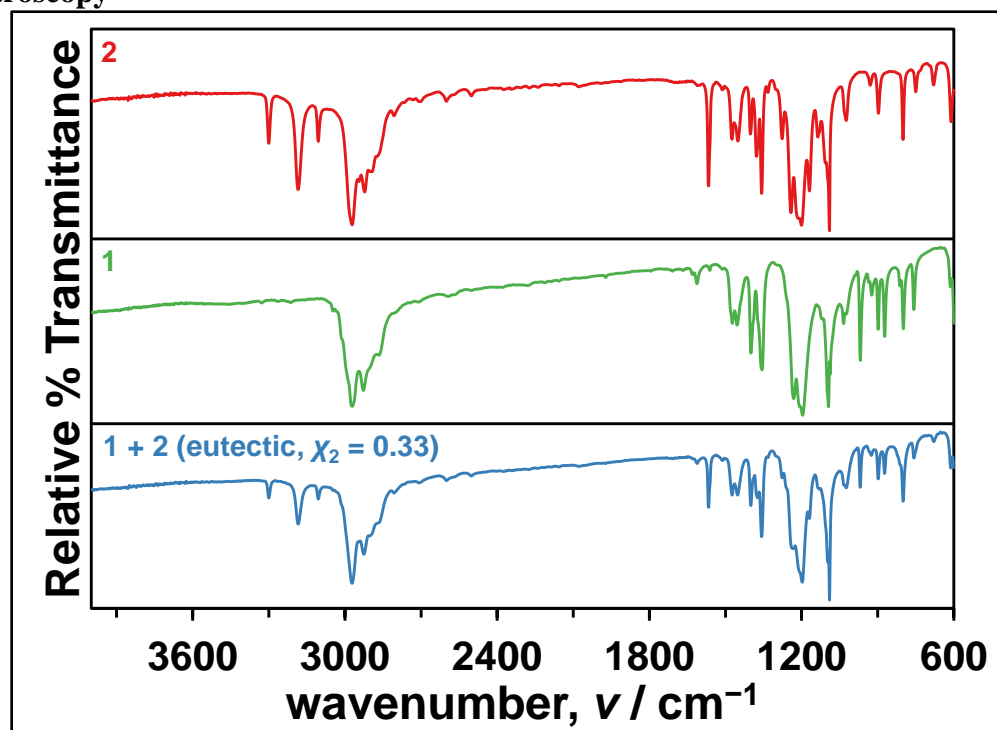


Figure S6: IR spectra of $(^t\text{BuN})_2\text{MoCl}_2 \cdot \text{dad}$ (**1**), $[(^t\text{BuN})_2\text{MoCl}(\mu\text{-Cl}) \cdot (^t\text{BuNH}_2)]_2$ (**2**), and a physical mixture of them (**2:12**, ground together in a mortar).

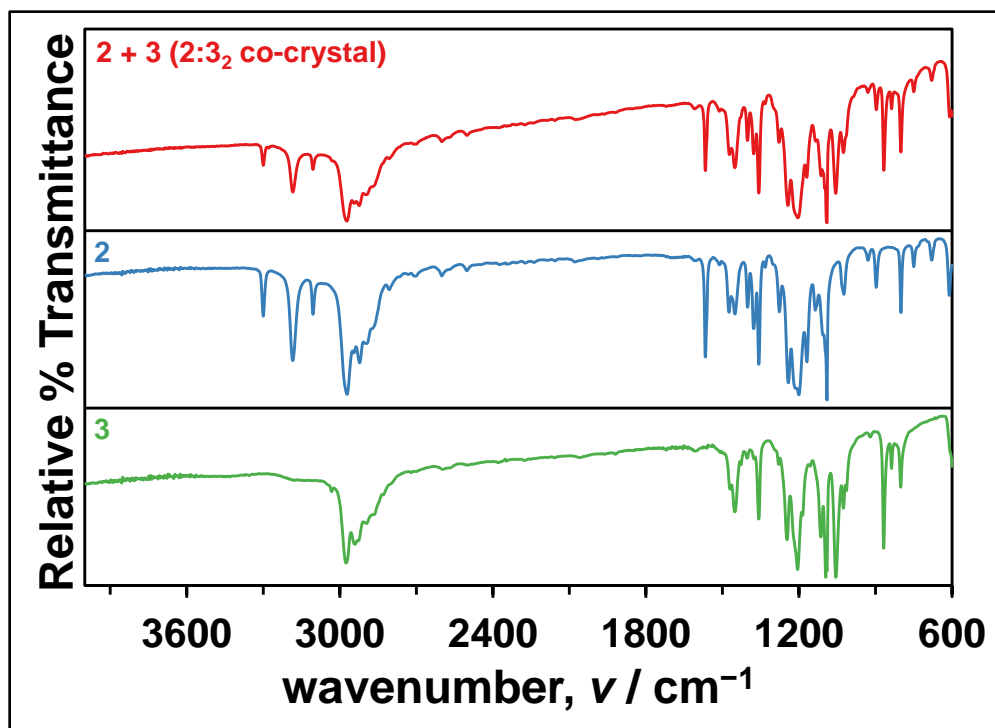


Figure S7: IR spectra of $[(^t\text{BuN})_2\text{MoCl}(\mu\text{-Cl})\cdot(^t\text{BuNH}_2)]_2$ (**2**), $(^t\text{BuN})_2\text{MoCl}_2\cdot\text{dme}$ (**3**), and a physical mixture of them (**2:3**₂, ground together in a mortar).

Powder X-ray Diffraction

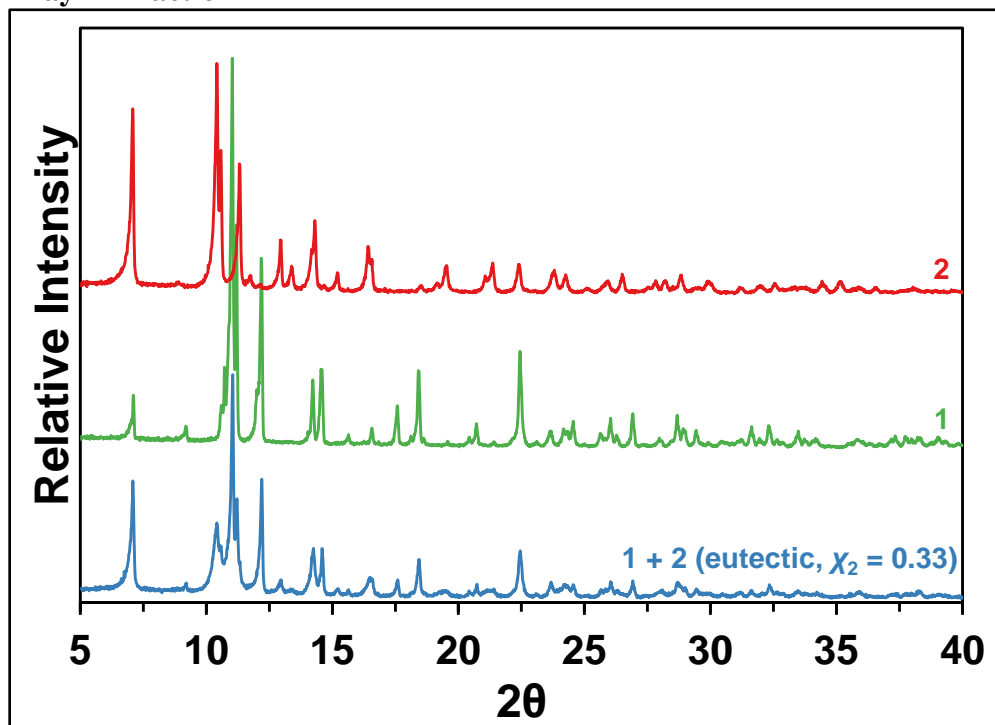


Figure S8: Powder diffraction patterns of $(^t\text{BuN})_2\text{MoCl}_2\cdot\text{dad}$ (**1**), $[(^t\text{BuN})_2\text{MoCl}(\mu\text{-Cl})\cdot(^t\text{BuNH}_2)]_2$ (**2**), and a physical mixture of them (**2:1**₂, ground together in a mortar).

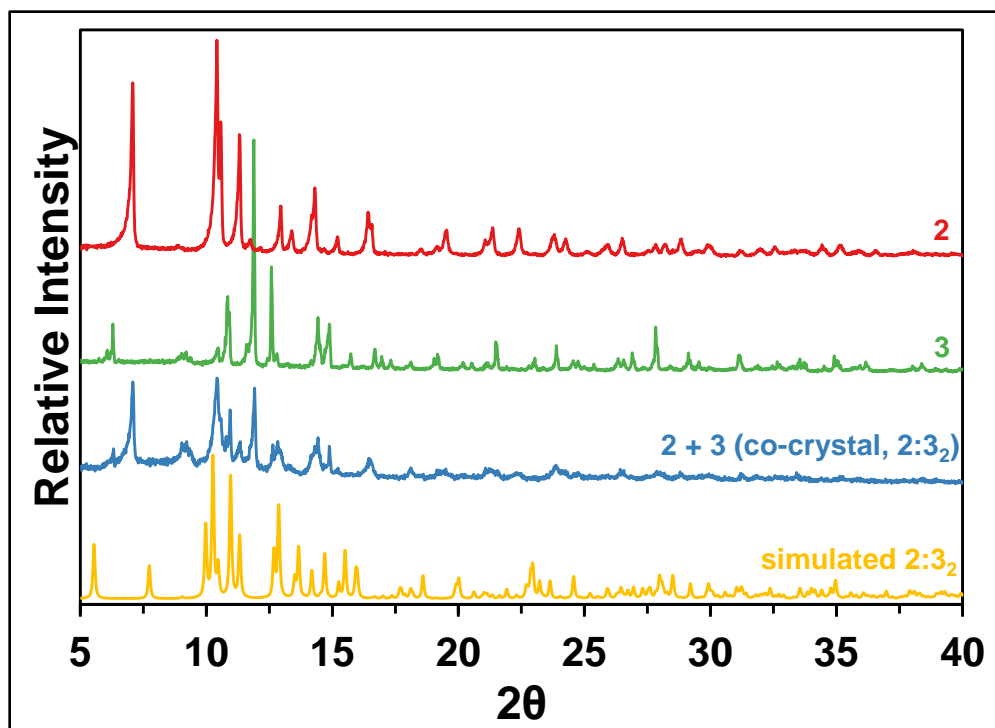


Figure S9: Powder diffraction patterns of $[(^t\text{BuN})_2\text{MoCl}(\mu\text{-Cl})\cdot(^t\text{BuNH}_2)_2]_2$ (**2**), $(^t\text{BuN})_2\text{MoCl}_2\cdot\text{dme}$ (**3**), a physical mixture of them (**2:3₂**, ground together in a mortar), and a simulated diffractogram from the single-crystal structure of **2:3₂**.

Electrostatic Potential Maps

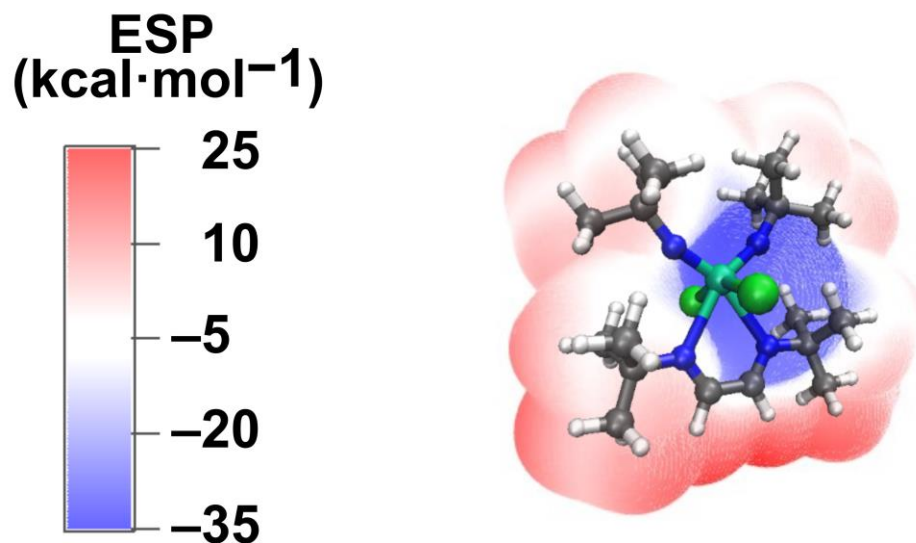


Figure S10: Electrostatic potential for **1**. ESP values are mapped onto a 0.001 au isosurface.

X-Ray Crystallography

The crystal chosen was attached to the tip of a MicroLoop with paratone-N oil. Measurements were made on a Bruker D8 VENTURE diffractometer equipped with a PHOTON III CMOS detector using monochromated Mo K α radiation ($\lambda = 0.71073 \text{ \AA}$) from an Incoatec microfocus sealed tube at 125 K [10]. The initial orientation and unit cell were indexed using a least-squares analysis of the reflections collected from a 180° phi-scan, 3 seconds per frame and 1° per frame. For data collection, a strategy was calculated to maximize data completeness and multiplicity, in a reasonable amount of time, and then implemented using the Bruker Apex 3 software suite [10]. The data were collected with appropriate frame times (given below) and the crystal to detector distance was set to 5 cm, except for **3** where a 4 cm distance was used. Cell refinement and data reduction were performed with the Bruker SAINT [11] software, which corrects for beam inhomogeneity, possible crystal decay, Lorentz and polarisation effects. A multi-scan absorption correction was applied (SADABS [12]). The structures were solved using SHELXT-2014 [13] and were refined using a full-matrix least-squares method on F^2 with SHELXL-2018 [13]. The refinements were generally unremarkable. The non-hydrogen atoms were refined anisotropically. The hydrogen atoms bonded to carbon were included at geometrically idealized positions and were refined on a riding model. The isotropic thermal parameters of these hydrogen atoms were fixed at $1.2U_{eq}$ of the parent carbon atom or $1.5U_{eq}$ for methyl hydrogens. In **2:3₂** the positions of the hydrogen atoms bonded to nitrogen were located in a near final Fourier difference map. They were allowed to refine isotropically with a weak restraint added to keep the two bond lengths similar and with $U_{iso}H(N)$ equal to $1.5U_{eq}(N)$. In **4:3** the hydrogen atoms bonded to nitrogen were not observed in a near final Fourier difference map. Instead, they were placed in geometrically reasonable positions and allowed to ride on the nitrogen atom to which they were bonded with $U_{iso}H$ equal to $1.5 U_{eq}N$.

2:3₂ CCDC 2214328 30 sec / 1 degree

Data was collected and integrated to a resolution of 0.70 \AA ($\theta_{max} = 30.51^\circ$). One reflection (1 0 1) was removed from the final refinement as it was partially obscured by the backstop during data collection.

One of the *tert*-butyl groups on the dimer was found to be disordered. Its atoms were split over two sets of positions, with the geometry of each part restrained to be similar using a SAME instruction during the refinement. The occupancies of the two parts refined to 58(1) and 42 %, respectively. The atomic displacement parameters of the carbon atoms in the disordered group were restrained to be similar, as were its N-C distances. In addition, one of the carbon atoms in each part of the *tert*-butyl group was found to lie on the same position, so it was constrained to have identical coordinates and atomic displacement parameters.

The crystal was found to be a composite of two different neutral compounds present in a ratio of 2:1(monomer to dimer). The structures of both of the neutral compounds have previously been reported, the monomer, $C_{12}H_{28}Cl_2MoN_2O_2$, by the Barry group [14] and the dimer,

C₂₄H₅₈Cl₄Mo₂N₆, by Chiu et al. [2]. Both constituents appear to have geometries similar to those found for the pure compounds in the solid state.

4:3 CCDC 2214329 60 sec / 2 degrees

Data was integrated to a maximum θ angle of 26.51° (0.80 Å resolution); all of this data was used in the refinement.

The structure was found to crystallize in the Triclinic, centrosymmetric space group *P*-1, with one complete Mo monomer and one complete Mo dimer is the asymmetric unit. The Mo monomer was found to contain a large amount of structural disorder; essentially everything except the 1,2-dimethoxyethane ligand was found to be disordered. This was modelled with a two part disorder with the occupancies of the atoms in the two parts set to (after refining to) 50 %. The two parts were restrained to have similar geometries and the atoms of the same type in parts A and B were constrained to have similar atomic displacement parameters. All of the terminal Mo-Cl bond lengths in the structure were restrained to be similar. Bonds between ordered and disordered atoms in the structure were restrained to be of similar lengths. Enhanced rigid bond restraints were placed over the entire structure.

The Mo dimer was found to contain two substitutionally different Mo centers, bridged by two common Cl atoms. The first center is bonded to three N(*t*-butyl) groups and one terminal Cl while the second is bonded to only two N(*t*-butyl) groups and two terminal Cl atoms. One N(*t*-butyl) group on each Mo center was observed to be significantly bent, with long Mo-N bond lengths; two hydrogen atoms were placed geometrically on the N atoms of these groups. The Mo dimer was also found to be significantly disordered. On Mo1 the *t*-butyl groups of two of the N(*t*-butyl) ligands were split over two positions, while for the second half of the dimer everything including Mo2 was modelled with a two part disorder. In addition, one of the bridging Cl atoms (but not the other) was observed to take two positions in the Fourier maps and was split into two parts. Refinement of disorder in the dimer was handled as described above for the monomer.

Only a few crystals of this compound were located in the sample and none of them were of good quality. The crystal used was the best one that could be found. As a result of the poor quality of the crystal, the resolution of the collected data was lower than expected. A number of checkcif alerts remained after the final refinement. In particular, one level B alert, Low Bond Precision on C-C Bonds, resulted from the large amount of disorder in the structure and the poor quality of the crystal used. The less than desirable quality of the data set also resulted in a few lower level checkcif alerts that also could not be resolved, including the final values of R1 and wR2 being higher than normal.

Data was collected with the resolution set to 0.65 Å and integrated to a maximum resolution of 0.60 Å ($\theta_{\max} = 36.31^\circ$). All of this data was used in the refinement of the structure.

The structure was found to crystallize in the non-centrosymmetric space group $R3c$. The Flack parameter was calculated to be -0.021(28) by classical fit to all intensities and -0.026(7) from 3632 selected quotients (Parsons' method). This was substantiated by calculation of the Hooft parameter using the program Platon [15]; it was determined to be -0.029(6). All of this suggests that the correct absolute configuration has been refined.

Note: This is the second polymorph determined for this compound. The first has an orthorhombic unit cell ($Pbca$ and $Z = 8$) with dimensions at 125 K of $a = 9.8388(9)$, $b = 12.4644(12)$ and $c = 29.816(3)$ Å and a volume of 3656.4(6) Å³ [15].

Table S1: Crystal data and structure refinement details.

	2:3₂	4:3	3
Identification code	2214328	2214329	2214327
CCDC deposit number	2214328	2214329	2214327
Empirical formula	C ₂₄ H ₅₇ Cl ₄ Mo ₂ N ₅ O ₂	C ₃₂ H ₇₇ Cl ₇ Mo ₃ N ₇ O ₂	C ₁₂ H ₂₈ Cl ₂ MoN ₂ O ₂
Formula weight	781.42	1127.97	399.20
Crystal system	Triclinic	Triclinic	Trigonal
Space group	<i>P</i> -1	<i>P</i> -1	<i>R</i> 3 <i>c</i> : H
Unit cell dimensions (Å and °)	<i>a</i> = 9.9569(4) <i>b</i> = 11.9148(5) <i>c</i> = 16.1787(7) α = 82.1846(17) β = 81.8216(16) γ = 74.5167(15)	<i>a</i> = 11.6961(18) <i>b</i> = 15.988(3) <i>c</i> = 16.238(3) α = 113.368(5) β = 108.738(5) γ = 97.767(5)	<i>a</i> = 27.6725(6) <i>b</i> = 27.6725(6) <i>c</i> = 12.4913(4) α = 90 β = 90 γ = 120
Volume (Å ³)	1821.20(13)	2516.4(7)	8283.9(4)
<i>Z</i>	2	2	18
Density (calculated, Mg/m ³)	1.425	1.489	1.440
Absorption coefficient (mm ⁻¹)	1.009	1.142	1.003
F(000)	808	1158	3708
Crystal size (mm ³)	0.143x0.137x0.045	0.128x0.074x0.050	0.138x0.065x0.040
Theta range of data (°)	2.085 to 30.508	1.893 to 26.511	2.550 to 36.310
Index ranges (<i>h</i> , <i>k</i> , <i>l</i>)	-14/14, -17/17, -23/23	-14/14, -20/19, -20/20	-46/29, -45/44, -20/20
Reflections collected	113051	116258	96178
Independent reflections	11093	10357	8752
R(int)	0.0472	0.0845	0.0330
Completeness to 25.242° (%)	99.9	100.0	99.9
Max. and min. transmission	0.7465 and 0.6842	0.0151 and 0.0030	0.0601 and 0.0239
Data / restraints / parameters	11093 / 32 / 386	10357 / 1414 / 775	8752 / 1 / 180
Goodness-of-fit on F ²	1.060	1.184	1.165
Final R indices [<i>I</i> >2σ(<i>I</i>)]	R1 = 0.0436 wR2 = 0.0814	R1 = 0.1420 wR2 = 0.3059	R1 = 0.0232 wR2 = 0.0424
R indices (all data)	R1 = 0.0666 wR2 = 0.0978	R1 = 0.1582 wR2 = 0.3130	R1 = 0.0352 wR2 = 0.0489
Absolute structure parameter	n.a.	n.a.	-0.026(7)
Largest diff. peak and hole (e.Å ⁻³)	1.420 and -1.428	1.418 and -1.557	0.633 and -0.711

Table S2: N-H...Cl hydrogen bonds in the structures studied [\AA and $^\circ$]. All identified contacts less than the sum of the van der Waals radii + 0.2 \AA , including intramolecular contacts.

D-H...A	d(D-H)	d(H...A)	d(D...A)	<(DHA)
2:3₂				
N(3)-H(1N3)...Cl(1)#1	0.89(3)	2.53(3)	3.412(3)	172(4)
N(3)-H(1N3)...Cl(2)#1	0.89(3)	2.80(4)	3.206(3)	109(3)
N(3)-H(2N3)...Cl(4) ^a	0.90(3)	3.22(3)	4.059(3)	157(3)
4:3				
N(3)-H(3NA)...Cl(6A)	0.88	2.65	3.51(3)	167.6
N(3)-H(3NA)...Cl(6B)	0.88	2.80	3.68(3)	173.1
N(3)-H(3NB)...Cl(4A)	0.88	2.71	3.575(18)	168.4
N(3)-H(3NB)...Cl(4B)	0.88	2.51	3.380(17)	168.2
N(3)-H(3NB)...Cl(1B)	0.88	2.76	3.09(2)	103.7
N(3)-H(3NB)...Cl(2)	0.88	2.61	2.971(16)	105.4
N(5A)-H(5NA)...Cl(7A)#2	0.88	2.87	3.71(4)	160.2
N(5A)-H(5NA)...Cl(7B)#2	0.88	2.63	3.48(4)	163.0
N(5A)-H(5NA)...Cl(5A)	0.88	2.74	3.09(4)	104.8
N(5A)-H(5NB)...Cl(2)	0.88	2.92	3.18(3)	99.3
N(5A)-H(5NB)...Cl(3)	0.88	2.58	3.46(3)	170.5
N(5B)-H(5NC)...Cl(7B)#2	0.88	2.99	3.84(4)	162.2
N(5B)-H(5NC)...Cl(5A)	0.88	2.46	2.87(4)	109.0
N(5B)-H(5NC)...Cl(5B)	0.88	2.75	3.09(4)	104.5
N(5B)-H(5NC)...Cl(2)	0.88	2.82	2.88(3)	84.6
N(5B)-H(5ND)...Cl(3)	0.88	2.58	3.46(3)	178.6
N(5B)-H(5ND)...Cl(1A)	0.88	2.56	2.86(3)	100.7
N(5B)-H(5ND)...Cl(2)	0.88	2.61	2.88(3)	98.6

Symmetry transformations used to generate equivalent atoms:

#1 -x,-y+1,-z+1 #2 -x+2,-y+1,-z+1

(a) This intramolecular interaction is slightly longer than the cut off limit chosen but it is the only contact made by N3-H2N3.

Table S3: C-H...Acceptor Hydrogen bonds for **2:3₂** [\AA and $^\circ$]. All identified contacts less than the sum of the van der Waals radii + 0.2 \AA , including all intramolecular contacts with angles greater than 110° .

D-H...A	d(D-H)	d(H...A)	d(D...A)	<(DHA)
C(2B)-H(2F)...Cl(4)	0.98	3.00	3.959(16)	168.1
C(3A)-H(3A)...Cl(4)	0.98	2.85	3.826(11)	174.0
C(3B)-H(3E)...Cl(3)#2	0.98	3.13	4.040(13)	155.7
C(4B)-H(4D)...Cl(1)	0.98	3.12	3.852(4)	132.9
C(7)-H(7A)...Cl(1)	0.98	3.07	3.678(6)	121.1
C(10)-H(10C)...Cl(4)	0.98	3.03	3.947(4)	156.1
C(11)-H(11A)...Cl(4)	0.98	3.12	4.021(4)	152.7
C(11)-H(11C)...Cl(1)#1	0.98	3.09	3.890(4)	139.7
C(12)-H(12A)...Cl(2)#1	0.98	3.14	3.621(4)	112.0
C(13)-H(13A)...Cl(2)	0.99	2.99	3.534(4)	115.4
C(13)-H(13A)...Cl(4)	0.99	2.87	3.369(4)	111.9
C(14)-H(14A)...Cl(3)	0.99	3.02	3.455(4)	108.2
C(14)-H(14B)...Cl(1)#1	0.99	2.89	3.792(4)	152.5
C(15)-H(15A)...Cl(4)	0.98	2.92	3.425(4)	113.1
C(15)-H(15C)...Cl(1)#3	0.98	3.02	3.677(4)	125.5
C(16)-H(16A)...Cl(3)	0.98	2.84	3.332(4)	111.7
C(16)-H(16C)...Cl(1)#1	0.98	2.90	3.804(4)	153.1
C(8)-H(8B)...O(1)#4	0.98	2.96	3.890(6)	158.1
C(11)-H(11A)...O(2)	0.98	2.87	3.611(5)	132.7
C(10)-H(10A)...N(2)	0.98	2.87	3.634(5)	134.9
C(12)-H(12C)...N(2)	0.98	2.61	3.409(5)	139.3
C(15)-H(15B)...N(4)	0.98	2.77	3.250(5)	110.6
C(16)-H(16B)...N(5)	0.98	2.85	3.358(4)	112.9
C(24)-H(24C)...C(19)#5	0.98	2.94	3.743(6)	139.4

Symmetry transformations used to generate equivalent atoms:

#1 -x,-y+1,-z+1 #2 x,y+1,z #3 -x+1,-y+1,-z+1 #4 x-1,y+1,z #5 -x+1,-y+1,-z

(a) This intermolecular interaction is slightly longer than the cut off limit chosen but it is the only contact accepted by O2.

Table S4: C-H...H-C interactions for **2:3₂** [Å and °]. All identified contacts less than the sum of the van der Waals radii + 0.2 Å, including intramolecular contacts.

D-H...A	d(D-H)	d(H...A)	d(D...A)	<(DHA)
C(2B)-H(2E)...H(12A)-C(12)#1	0.98	2.46	3.049(12)	118.5
C(2B)-H(2E)...H(12B)-C(12)#1	0.98	2.59	3.336(19)	133.1
C(3B)-H(3D)...H(10A)-C(10)	0.98	2.61	3.01(3)	104.6
C(3B)-H(3D)...H(10C)-C(10)	0.98	2.44	3.26(3)	141.2
C(3B)-H(3F)...H(6A)-C(6)	0.98	2.26	3.22(3)	166.9
C(4A)-H(4B)...H(8A)-C(8)#1	0.98	2.60	3.522(8)	156.1
C(4A)-H(4C)...H(7B)-C(7)#2	0.98	2.47	3.25(3)	137.0
C(4B)-H(4D)...H(7B)-C(7)#2	0.98	2.57	3.25(3)	126.5
C(4B)-H(4E)...H(16A)-C(16)#3	0.98	2.54	3.419(17)	150.0
C(7)-H(7C)...H(4A)-C(4A)	0.98	2.38	3.313(8)	158.1
C(7)-H(7C)...H(4D)-C(4B)	0.98	2.34	3.200(7)	145.6
C(7)-H(7C)...H(7A)-C(7)#2	0.98	2.54	3.177(11)	122.6
C(8)-H(8C)...H(13B)-C(13)#4	0.98	2.55	3.420(6)	148.2
C(8)-H(8C)...H(14B)-C(14)#4	0.98	2.56	3.462(6)	152.3
C(10)-H(10A)...H(6C)-C(6)	0.98	2.31	3.04(4)	131.1
C(12)-H(12B)...H(23B)-C(23)#5	0.98	2.60	3.55(4)	166.4
C(12)-H(12C)...H(6C)-C(6)	0.98	2.59	3.329(14)	132.4
C(12)-H(12C)...H(8A)-C(8)	0.98	2.39	3.310(15)	155.6
C(14)-H(14A)...H(4E)-C(4B)#6	0.99	2.58	3.435(5)	145.1
C(15)-H(15B)...H(18A)-C(18)	0.98	2.42	3.39(3)	166.7
C(16)-H(16B)...H(24A)-C(24)	0.98	2.56	3.500(19)	159.7
C(18)-H(18C)...H(6B)-C(6)#7	0.98	2.37	3.140(16)	134.6
C(19)-H(19A)...H(23A)-C(23)	0.98	2.61	3.52(4)	154.4
C(19)-H(19B)...H(10B)-C(10)#8	0.98	2.50	3.389(12)	150.2
C(20)-H(20A)...H(22C)-C(22)#9	0.98	2.54	3.272(14)	131.3
C(20)-H(20C)...H(23C)-C(23)	0.98	2.12	3.06(2)	160.0
C(24)-H(24A)...H(18B)-C(18)#10	0.98	2.44	3.291(12)	145.4

Symmetry transformations used to generate equivalent atoms (both C and H of the acceptor):

#1 x+1, y, z #2 -x, -y+2, -z+1 #3 x, y+1, z #4 -x, -y+1, -z+1 #5 -x, -y+1, -z
 #6 x, y-1, z #7 x+1, y-1, z #8 -x+1, -y+1, -z #9 -x+1, -y, -z #10 x-1, y, z

Analysis of the Intermolecular Interactions Found in the Crystal Structure Determination of **2:3₂**

The structure is centrosymmetric with one half of the dimer and one monomer unique in the asymmetric unit. However, the logical unit to consider comprises one complete dimer and two monomers. The second half of the dimer and the second monomer molecule are generated using the symmetry operation $(-x, -y+1, -z+1)$.

The major acceptor group of the intermolecular interactions in this structure are the Cl atoms. The dimer contains one unique terminal Cl (Cl1) and one unique bridging Cl atom (Cl2). The monomer contains two terminal Cl atoms (Cl3 and Cl4). Other possible “traditional” acceptor atoms in the structure are oxygen (O1 and O2 in the monomer) and nitrogen atoms in both units. The monomer has two unprotonated nitrogen atoms (N4 and N5) but the dimer has three unique nitrogen atoms that fall into two groups (N1 and N2 that are unprotonated and N3 which has H1N3 and H2N3 bonded to it). There are carbon and hydrogen atoms that can interact but there are only alkyl groups in both the dimer and monomer so there is no chance of stacking or other types of π -interactions being formed. The donor atoms in the structure begin with the aforementioned H1N3 and H2N3 of the dimer. Beyond that there are only alkyl C-H groups in both the monomer and dimer. The only real difference between alkyl groups occurs in the monomer where the C-H groups of the coordinated dme ligand are chemically different from the *t*-Bu groups; in the dimer there are only *t*-Bu groups. There are many more C-H donor groups than available acceptors in the structure. This means that to form suitable interactions, many groups will be reduced to forming C-H...H-C contacts.

The positions of H1N3 and H2N3 were refined and both N3-H1N3 and N3-H2N3 form hydrogen bonds with Cl acceptors. N3-H1N3 forms a short/strong and linear intramolecular hydrogen bond with Cl1 on the opposite side of the dimer; it also has a weak second component to the related Cl2 center in the same dimer. The formation of this strong interaction leaves H2N3 with fewer options. The only HB that it forms is very long (well beyond the sum of the van der Waals radii) but it is intermolecular, and quite linear ($157(3)^\circ$), joining the monomer and dimer via Cl4; there are two such interactions per dimer.

The C-H hydrogen bonds also form predominantly with Cl atoms as the acceptors. In addition to these, two C-H...O (both intermolecular), one C-H...C (intermolecular but between two interacting methyl groups) and four C-H...N (all intramolecular) hydrogen bonds were identified. Their contributions are minor relative to the much larger number of C-H...Cl hydrogen bonds identified. A total of 17 C-H...Cl HBs were identified in the search. These can be divided in a number of different ways:

(i) Cl Acceptors: In the dimer Cl1, the terminal Cl, interacts with a total of 6 C-H groups, forming 3 intramolecular and 3 intermolecular bonds. In contrast, Cl2, the bridging Cl atom, interacts with only two C-H groups, one inter- and one intra-molecular. So, in the dimer, the terminal Cl center is a much better hydrogen bond acceptor than the bridging Cl2. In the monomer, Cl3 and Cl4 are both terminal. The molecule is quite symmetrical with Cl3 and Cl4 trans to each other and having similar arrangements to the other groups in the monomer as well. Despite this, Cl3 accepts only 3

hydrogen bonds, 1 intermolecular and 2 intramolecular, while Cl4 accepts twice as many, the total of 6 comprising 4 intermolecular and 2 intramolecular contacts (and Cl4 also accepts the long hydrogen bond to H2N3). The packing of the monomer relative to the dimer in the solid state must give Cl4 a geometric advantage in the formation of the C-H...Cl interactions. In total, the unique Cl atoms of the monomer participate in 8 hydrogen bonds while the Cl atoms of the unique half of one dimer participate in a total of 9 hydrogen bonds, a relatively even distribution.

(ii) Donor C-H Groups: In the monomer, the C-H donor atoms are located specifically in the region of the molecule containing the dme ligand (C13 to C16) and tend not to involve the *t*-Bu groups. Again, this results in (or is a consequence of) the dme end of the monomer being oriented towards the dimer in the crystal packing, favouring the formation of intermolecular C-H contacts of the monomer with the dimer. The monomer contributes 8 C-H donors to the list, 5 are intermolecular and 3 are intramolecular. The dimer contributes an almost equal number of unique C-H donor groups, 9, of which 5 are intermolecular and 4 are intramolecular, another relatively equal distribution. In the dimer all of the *t*-Bu groups have C-H groups that form hydrogen bonds; there appears to be no preference.

(iii) Dimer compared to Monomer: In the 17 interactions, there are 9 C-H...Cl HBs that occur between a dimer and a monomer molecule and all of these are (by definition) intermolecular in nature. There are 4 monomer...monomer contacts and 4 dimer...dimer interactions. Although these do not have to be so, all 8 are intramolecular contacts.

As mentioned above numerous C-H...H-C contacts form because of the lack of “better” acceptors in the molecules. A total of 27 such contacts, less than the sum of the van der Waals radii plus 0.2 Å and with angles of greater than 100°, were identified. For the intramolecular contacts there are obviously many that could be reported in every alkyl-containing group. The criteria used, limit those listed to the ones involving different alkyl groups. It should also be noted that each C-H...H-C contact can be reported in two different ways; every contact has been included only once, and is written in the direction which gives the larger C-H...H angle. The number of C-H...H-C contacts found is identical to the 27 N-H and C-H...acceptor hydrogen bonds discussed above, showing an even split between the two broad groups in the solid. Again, this ratio is likely determined by the number and type of available acceptors rather than anything more.

A total of 12 C-H...H-C intramolecular contacts were identified, 8 of which involved C-H groups only in the asymmetric unit of one dimer and 4 of which were only in the monomer. Almost all of these contacts involve only *t*-Bu C-H groups, even in the monomer. 15 intermolecular C-H...H-C contacts were located. 6 of these involved two different dimer molecules interacting and 2 involved interactions between two different monomers. The remaining 7 interactions are between a dimer and a monomer molecule. For the monomer, the interactions with the dimer involve a mixture of the dme and *t*-Bu C-H groups. However, the monomer...monomer contacts must occur on the opposite side of the molecule (away from the dimer) and thus involve only interactions between alkyl C-H groups. In the dimer all three *t*-Bu groups participate in both monomer...dimer and dimer...dimer intermolecular C-H...H-C contacts. However, the two *t*-Bu groups containing the methyl carbon atoms (C2 to C4 and C6 to C8) feature much more prominently than the third group (C10 to C12), which perhaps is sterically shielded.

If the usual hierarchical arrangement of hydrogen bonds and contacts is formed, one might envision the strong intramolecular N3-H1N3...Cl1 hydrogen bond being the most important. Once formed it would leave H2N3 looking for a contact, which it satisfies by forming a long intermolecular contact to Cl4 of a monomer. This would bring Cl4 into closer proximity to the dimer (relative to Cl3), in turn enabling it to accept a number of other C-H...Cl4 contacts from the dimer. This spatial arrangement of the monomer and dimer, orients the dme ligand on the monomer closest to the dimer and results in the formation of C-H...Cl and C-H...H-C monomer...dimer interactions predominantly from that location on the monomer. The same orientation means that when the monomer forms interactions from the *t*-Bu side, they are only with *t*-Bu groups on a second monomer molecule.

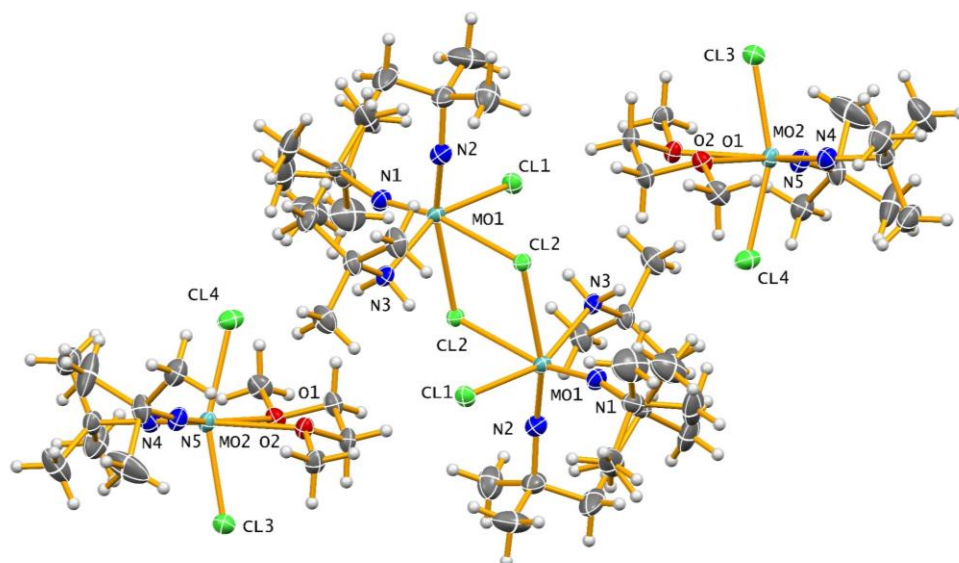


Figure S11: Solid-state structure of **2:3₂** with only the non-carbon heavy atoms labelled. The disorder has not been removed. Hydrogen atoms are included but have not been labelled. Thermal ellipsoids are drawn at the 50% probability level.

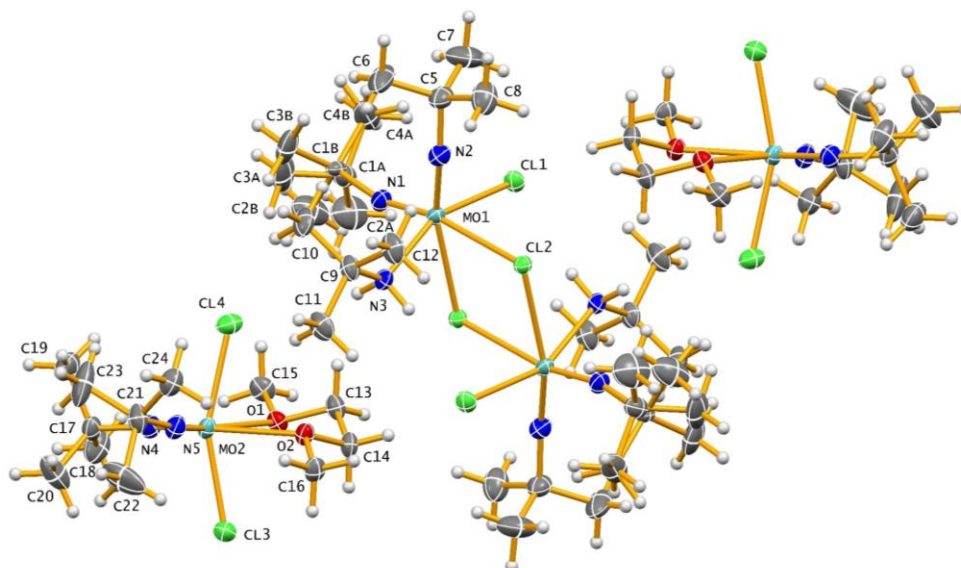


Figure S12: Solid-state structure of **2:3₂** with the unique heavy atoms labelled. The disorder has not been removed. Hydrogen atoms are included but have not been labelled. Thermal ellipsoids are drawn at the 50% probability level.

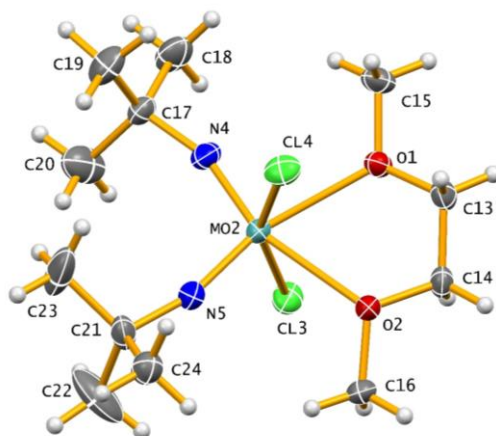


Figure S13: The monomer unit (**3**) of **2:3₂** with the heavy atoms labelled. Hydrogen atoms are included but are not labelled. Thermal ellipsoids are drawn at the 50% probability level.

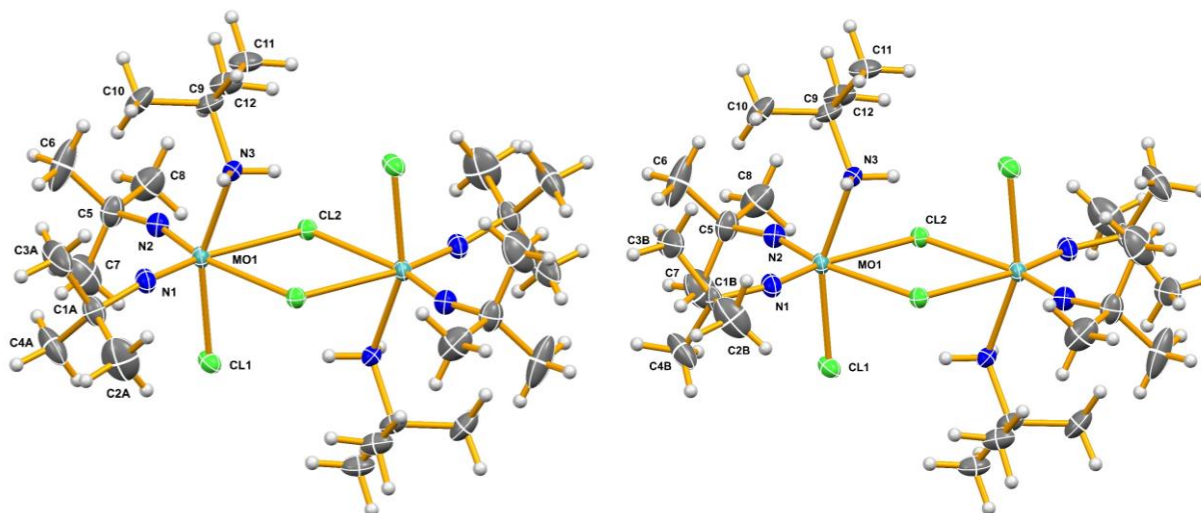


Figure S14: The disordered dimer unit (**2**) of **2:3₂** separated into two ordered parts with the heavy atoms labelled. Hydrogen atoms are included but have not been labelled. Thermal ellipsoids are drawn at the 50% probability level.

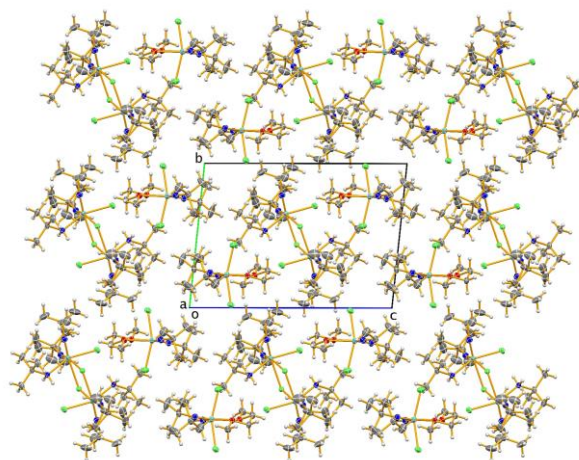


Figure S15: Solid-state packing diagram of **2:3₂** viewed in projection down the X-axis.

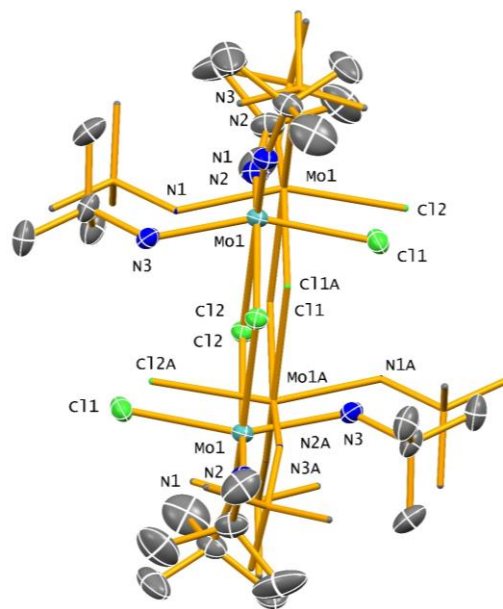


Figure S16: A view of the dimer (**2**) isolated in **2:3₂** (thermal ellipsoids) overlaid with the dimer reported by H.-T. Chiu et al. [ref. 2] (atomic coordinates accessed from CSD entry ZOBMIM [ref. 16]).

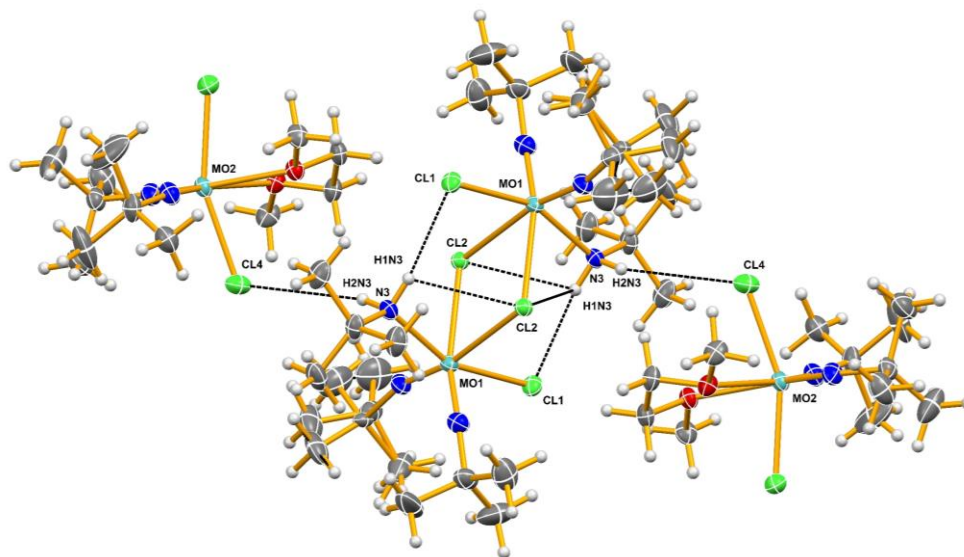


Figure S17: Selected N-H...Cl hydrogen bonds, both intra- and inter-molecular (dashed lines), in the solid-state structure of **2:3₂** (Table S2). Only those atoms directly involved in the contacts have been labelled.

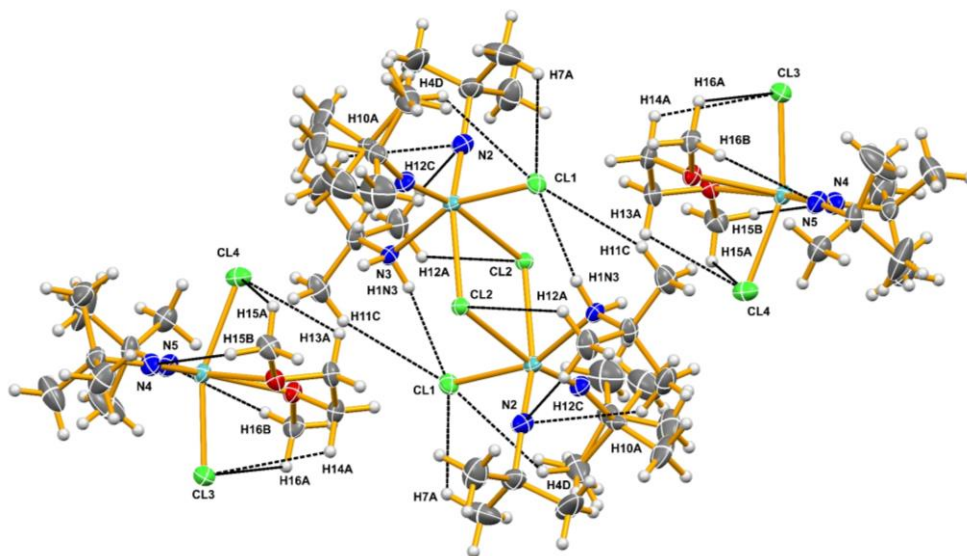


Figure S18: Selected intramolecular C-H...Cl and C-H...N interactions (below the sum of the Van der Waals radii + 0.2 Å; Tables S2 and S3; dashed lines) in the solid-state structure of **2:32**. The N-H...Cl hydrogen bond has also been included. Only those atoms directly involved in the contacts have been labelled.

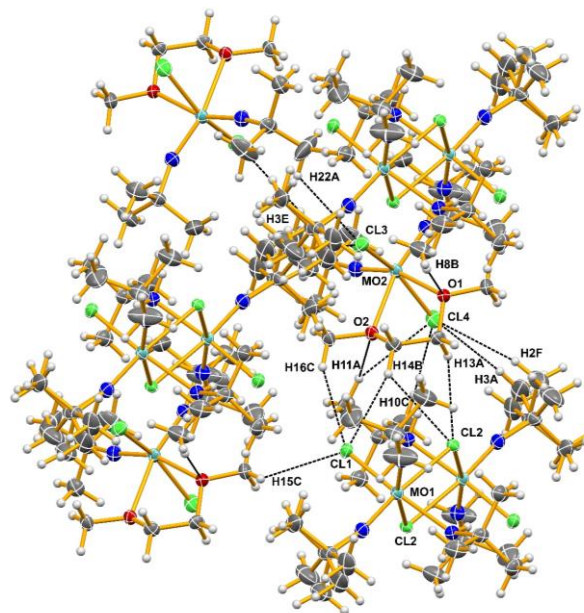


Figure S19: Selected intermolecular C-H...Cl and C-H...O interactions (below the sum of the Van der Waals radii + 0.2 Å; Tables S3; dashed lines) in the solid-state structure of **2:32**. Only the interactions to one monomer and to the unique half of one dimer have been included. Only those atoms directly involved in the contacts have been labelled.

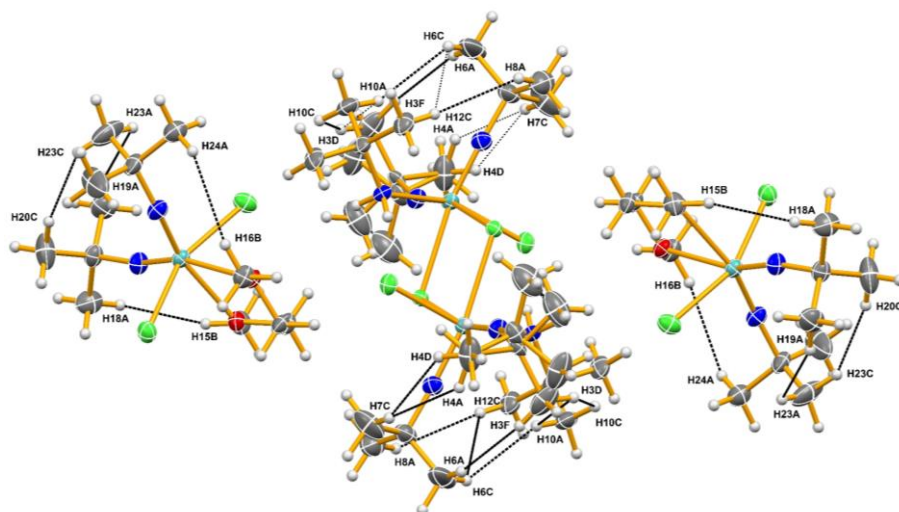


Figure S20: Selected intramolecular C-H...H-C interactions (below the sum of the Van der Waals radii + 0.2 Å; Tables S4; dashed lines) in the solid-state structure of **2:32**. Only those atoms directly involved in the contacts have been labelled.

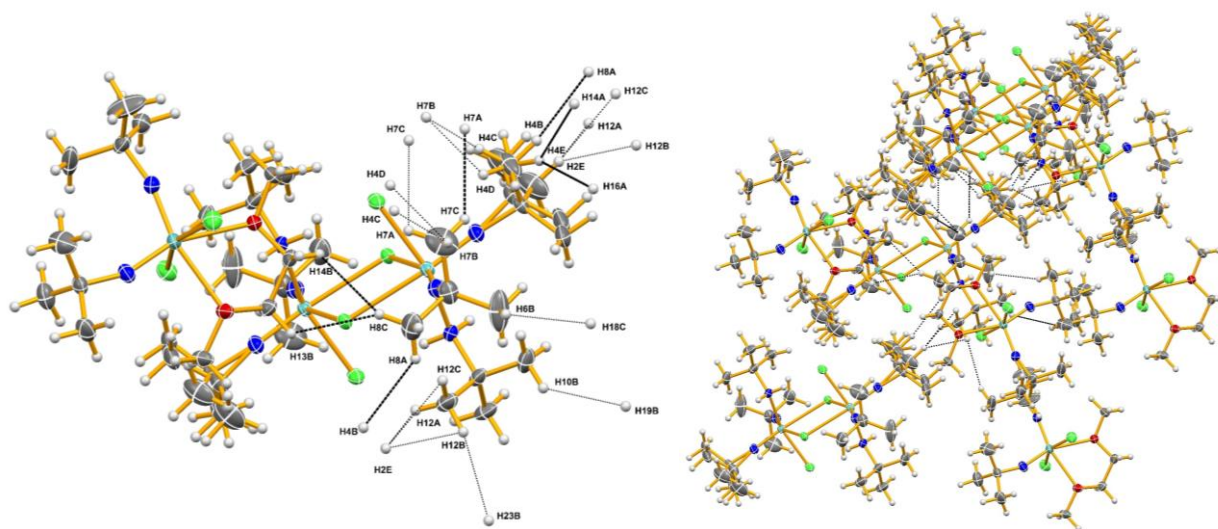


Figure S21: Selected intermolecular C-H...H-C interactions (below the sum of the Van der Waals radii + 0.2 Å; Tables S4; dashed lines) in the solid-state structure of **2:32**. Because of the complexity, the left diagram shows the correct labelling but only the hydrogen atom of the acceptor in the contact has been drawn, while the right diagram (shown in the same orientation) includes the full contacts but has not been labelled.

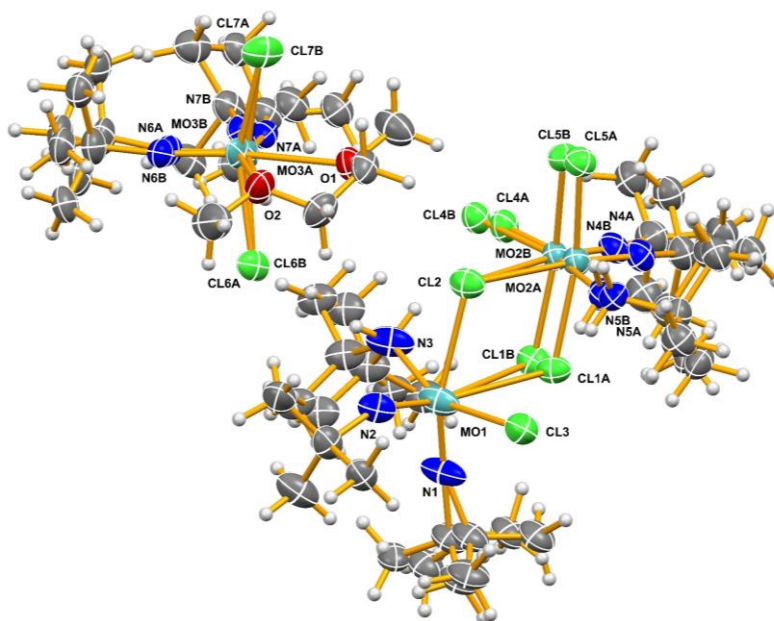


Figure S22: Solid-state structure of **4:3** with only the non-carbon heavy atoms labelled. The disorder has not been removed. Hydrogen atoms are included but have not been labelled. Thermal ellipsoids are drawn at the 50% probability level.

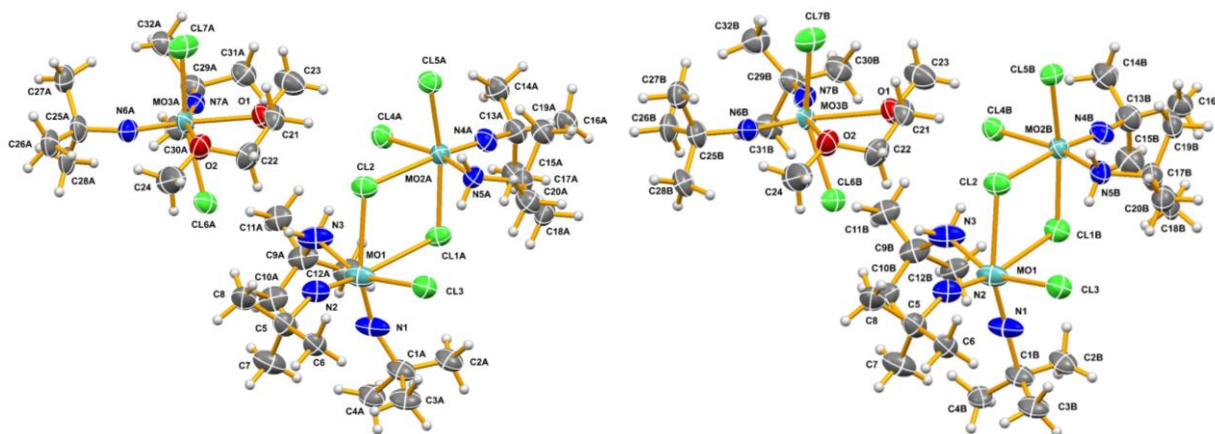


Figure S23: The disordered structure of **4:3** separated into two ordered parts, with the heavy atoms labelled. Hydrogen atoms are included but have not been labelled. Thermal ellipsoids are drawn at the 50% probability level.

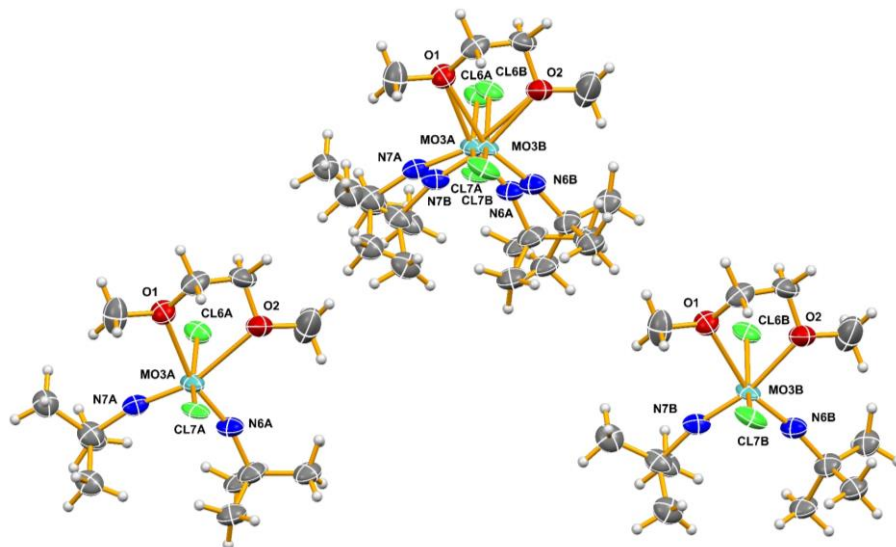


Figure S24: The two disordered parts of the monomer in **4:3** separated into two ordered parts, with the heavy atoms labelled. Hydrogen atoms are included but have not been labelled. Thermal ellipsoids are drawn at the 50% probability level.

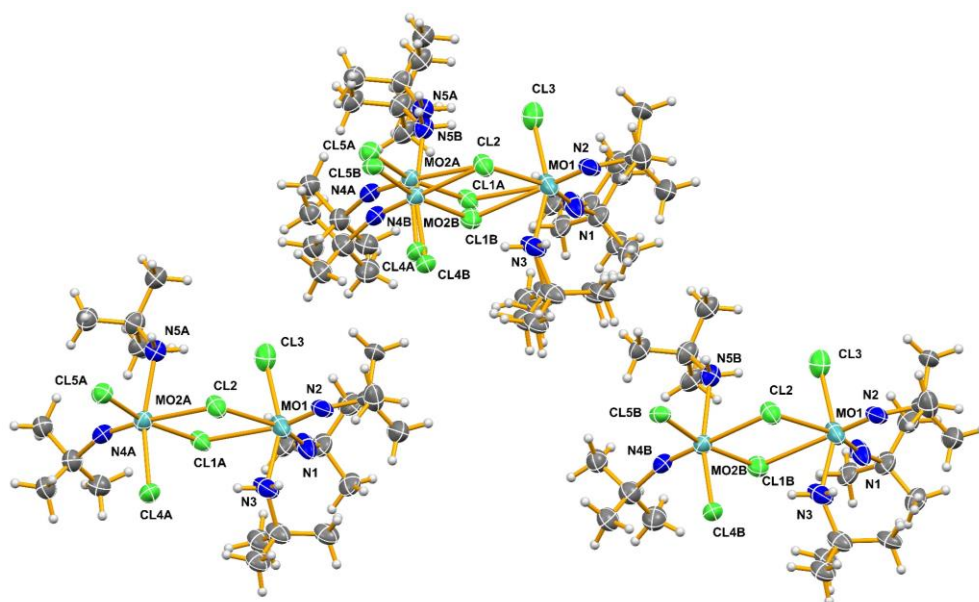


Figure S25: The two disordered parts of the dimer in **4:3** separated into two ordered parts, with the heavy atoms labelled. Hydrogen atoms are included but have not been labelled. Thermal ellipsoids are drawn at the 50% probability level.

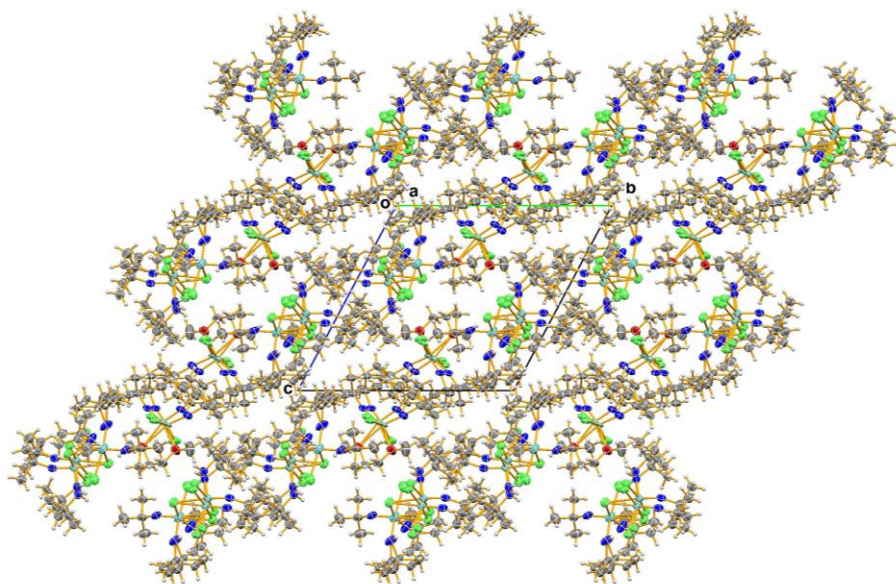


Figure S26: Solid-state packing diagram of **4:3** viewed in projection down the X-axis.

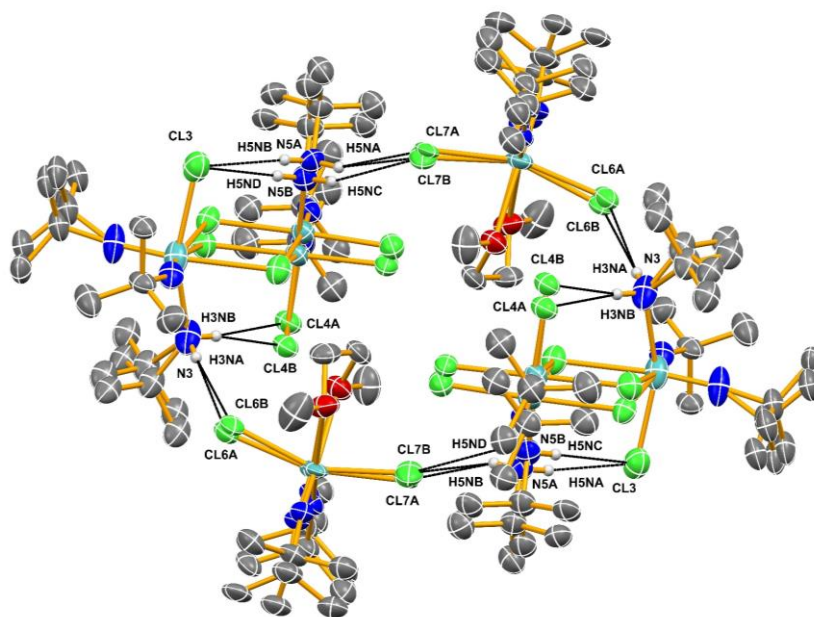


Figure S27: Selected N-H...Cl hydrogen bonds, both intra- and inter-molecular (dashed lines), in the solid-state structure of **4:3** (Table S2). Only those atoms directly involved in the contacts have been labelled.

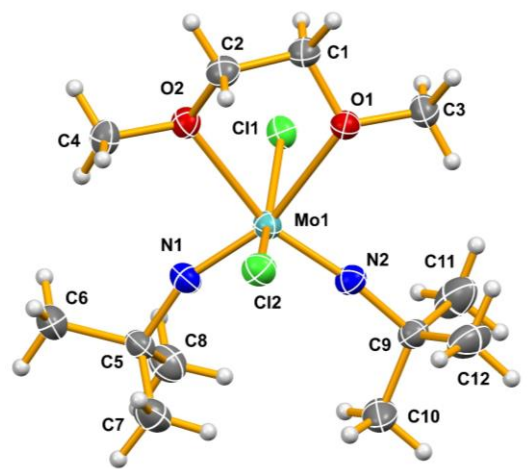


Figure S28: Solid-state structure of the new dme polymorph (**3**) with the heavy atoms labelled. Hydrogen atoms are included but have not been labelled. Thermal ellipsoids are drawn at the 50% probability level.

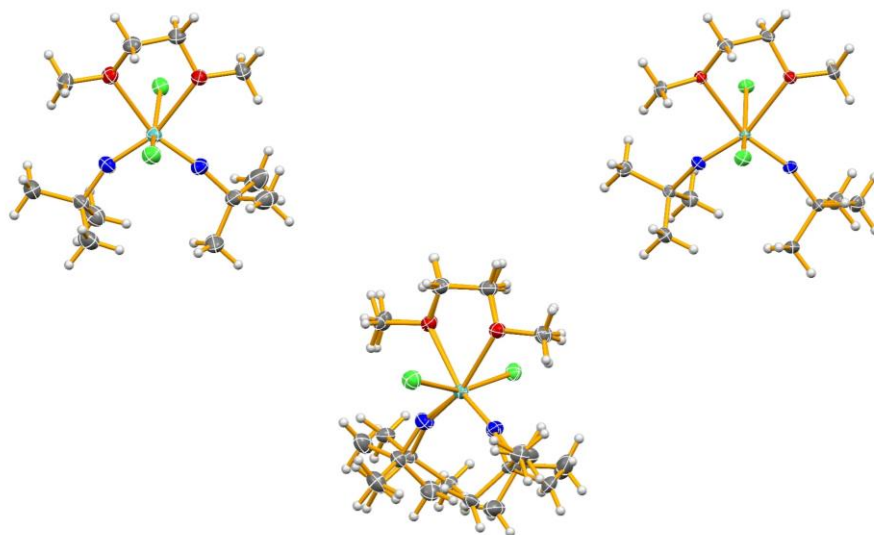


Figure S29: Solid-state structures of the two dme polymorphs. On the top left is the structure being reported here (**3**), on the right is the published structure [ref 14] and in the bottom middle the two structures have been overlaid. Hydrogen atoms are included. Thermal ellipsoids are drawn at the 50% probability level.

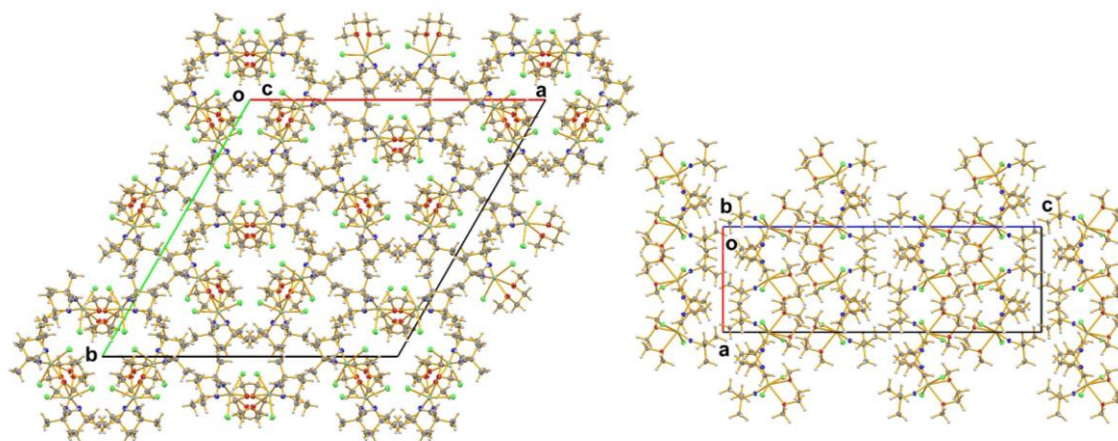


Figure S30: Packing diagrams of the two dme polymorphs viewed in projection. On the left is the structure being reported here (**3** - viewed down the Z-axis), on the right is the published structure (viewed down the Y-axis) [ref 15].

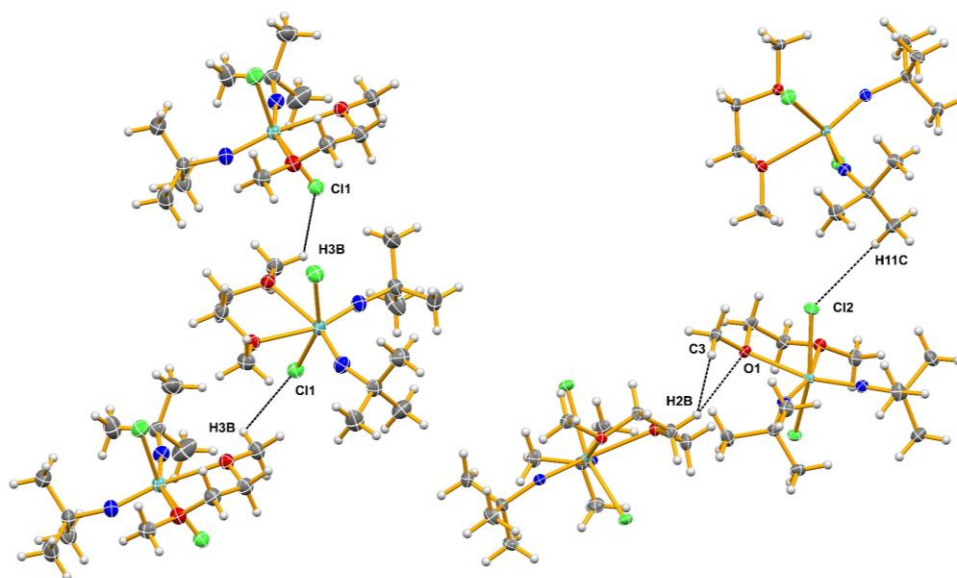
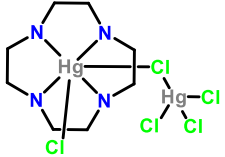
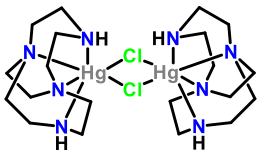
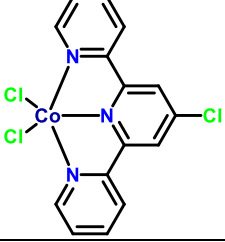
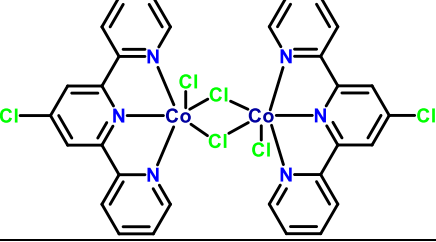
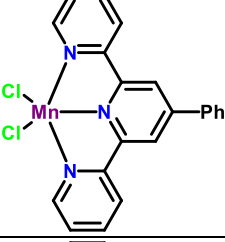
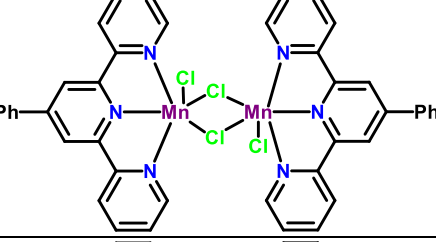
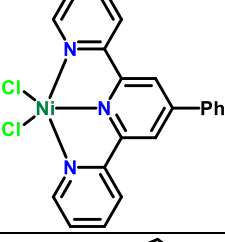
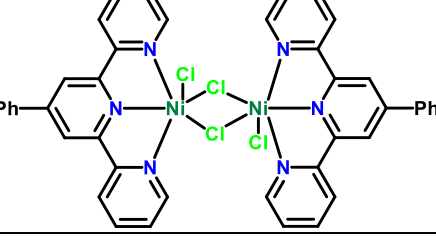
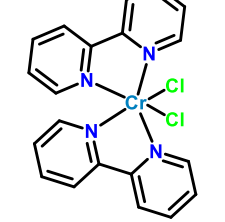
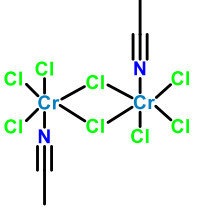
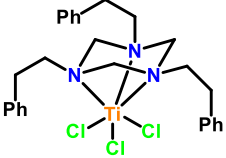
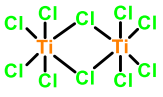


Figure S31: Selected intermolecular C-H...Acceptor interactions (A = N, O or Cl; less than the sum of the van der Waals radii) in the two dme polymorphs. On the left is the structure being reported here (**3**) and on the right is the published structure [ref 15].

Table S5: A search of the Cambridge Structural Database,¹⁶ performed on July 14, 2022, revealed the following crystal structures of co-crystals between a transition metal dimer (containing halides and nitrogen ligands) and a monomeric transition metal complex.

CCDC #	Component 1	Component 2	Ref.
1969561			[17]
1021672			[18]
935828			[19]
181882			[20]
810900			[21]
257784			[22]

References

- [1] M. A. Land, G. Bačić, K. N. Robertson and S. T. Barry, *Inorg. Chem.* 2022, **61**, 4980-4994.
- [2] H. -T. Chiu, G. -B. Chang, W. -Y. Ho, S. -H. Chuang, G. -H. Lee and S. -M. Peng, *J. Chinese Chem. Soc.* 1994, **41**, 755-761.
- [3] P. W. Dyer, V. C. Gibson, J. A. K. Howard, B. Whittle and C. Wilson, *J. Chem. Soc., Chem. Commun.* 1992, 1666-1668.
- [4] M. J. Frisch, G. W. Trucks, H. B. Schlegel, G. E. Scuseria, M. A. Robb, J. R. Cheeseman, G. Scalmani, V. Barone, G. A. Petersson, H. Nakatsuji, X. Li, M. Caricato, A. V. Marenich, J. Bloino, B. G. Janesko, R. Gomperts, B. Mennucci, H. P. Hratchian, J. V. Ortiz, A. F. Izmaylov, J. L. Sonnenberg, D. Williams-Young, F. Ding, F. Lipparini, F. Egidi, J. Goings, B. Peng, A. Petrone, T. Henderson, D. Ranasinghe, V. G. Zakrzewski, J. Gao, N. Rega, G. Zheng, W. Liang, M. Hada, M. Ehara, K. Toyota, R. Fukuda, J. Hasegawa, M. Ishida, T. Nakajima, Y. Honda, O. Kitao, H. Nakai, T. Vreven, K. Throssell, J. A. Montgomery, Jr., J. E. Peralta, F. Ogliaro, M. J. Bearpark, J. J. Heyd, E. N. Brothers, K. N. Kudin, V. N. Staroverov, T. A. Keith, R. Kobayashi, J. Normand, K. Raghavachari, A. P. Rendell, J. C. Burant, S. S. Iyengar, J. Tomasi, M. Cossi, J. M. Millam, M. Klene, C. Adamo, R. Cammi, J. W. Ochterski, R. L. Martin, K. Morokuma, O. Farkas, J. B. Foresman, and D. J. Fox, Gaussian 16 Revision A. 03. Gaussian, Inc., Wallingford CT, 2016.
- [5] (a) A. D. Becke, *Phys. Rev. A*, 1988, **38**, 3098-3100; (b) J. P. Perdew, *Phys. Rev. B*, 1986, **33**, 8822-8824.
- [6] F. Weigend and R. Ahlrichs, *Phys. Chem. Chem. Phys.* 2005, **7**, 3297-3305.
- [7] (a) S. Grimme, J. Antony, S. Ehrlich and H. Krieg, *J. Chem. Phys.* 2010, **132**, 154104; (b) S. Grimme, S. Ehrlich and L. Goerigk, *J. Comp. Chem.* 2011, **32**, 1456-1465.
- [8] T. Lu and F. Chen, *J. Comput. Chem.* 2012, **33**, 580-592.
- [9] W. Humphrey, A. Dalke and K. Schulten, *J. Molec. Graphics*, 1996, **14**, 33-38.
- [10] APEX 3 (Bruker, 2018) Bruker AXS Inc., Madison, Wisconsin, USA.
- [11] SAINT (Bruker, 2016) Bruker AXS Inc., Madison, Wisconsin, USA.
- [12] SADABS (Bruker, 2016) Bruker AXS Inc., Madison, Wisconsin, USA.
- [13] (a) G. M. Sheldrick, *Acta Cryst.* 2015, **A71**, 3-8; (b) G. M. Sheldrick, *Acta Cryst.* 2015, **C71**, 3-8.
- [14] M. A. Land, K. N. Robertson and S. T. Barry, *Organometallics*, 2020, **39**, 916-927.
- [15] A. L. Spek, *Acta Cryst.* 2009, **D65**, 148-155.
- [16] C. R. Groom, I. J. Bruno, M. P. Lightfoot and S. C. Ward, S.C. *Acta Cryst.* 2016, **B72**, 171-179.
- [17] A. L. Rheingold and E. S. Wong, CCDC 1969561: Experimental Crystal Structure Determination. *CSD Commun.* **2019**, DOI: 10.5517/ccdc.csd.cc243h70.
- [18] G. Zhang, J. Tan, Y. Z. Zhang, C. Ta, S. Sanchez, S. -Y. Cheng, J. A. Golen, and A. L. Rheingold, *Inorg. Chim Acta*, 2015, **435**, 147-152.
- [19] T. -H. Huang and M. -H. Zhang, *Inorg. Chim. Acta*, 2013, **408**, 91-95.
- [20] E. C. Constable, D. Phillips and P. R. Raithby, *Inorg. Chem. Commun.* 2002, **5**, 519-521.
- [21] L. J. Batchelor, M. Sander, F. Tuna, M. Helliwell, F. Moro, J. van Slageren, E. Burzuri, O. Montero, M. Evangelisti, F. Luis and E. J. L. McInnes, *Dalton Trans.* **2011**, **40**, 5278-5284.
- [22] R. D. Kohn, P. Kampe and G. Kociok-Kohn, *Eur. J. Inorg. Chem.* 2005, 3217-3223.